



This is a repository copy of *A general framework for the analysis and design of tubular linear permanent magnet machines.*

White Rose Research Online URL for this paper:
<http://eprints.whiterose.ac.uk/852/>

Article:

Wang, J.B., Jewell, G.W. and Howe, D. (1999) A general framework for the analysis and design of tubular linear permanent magnet machines. *IEEE Transactions on Magnetics*, 35 (3 (Par)). pp. 1986-2000. ISSN 0018-9464

<https://doi.org/10.1109/20.764898>

Reuse

Unless indicated otherwise, fulltext items are protected by copyright with all rights reserved. The copyright exception in section 29 of the Copyright, Designs and Patents Act 1988 allows the making of a single copy solely for the purpose of non-commercial research or private study within the limits of fair dealing. The publisher or other rights-holder may allow further reproduction and re-use of this version - refer to the White Rose Research Online record for this item. Where records identify the publisher as the copyright holder, users can verify any specific terms of use on the publisher's website.

Takedown

If you consider content in White Rose Research Online to be in breach of UK law, please notify us by emailing eprints@whiterose.ac.uk including the URL of the record and the reason for the withdrawal request.



eprints@whiterose.ac.uk
<https://eprints.whiterose.ac.uk/>

A General Framework for the Analysis and Design of Tubular Linear Permanent Magnet Machines

Jiabin Wang, *Member, IEEE*, Geraint W. Jewell, and David Howe

Abstract—A general framework for the analysis and design of a class of tubular linear permanent magnet machines is described. The open-circuit and armature reaction magnetic field distributions are established analytically in terms of a magnetic vector potential and cylindrical coordinate formulation, and the results are validated extensively by comparison with finite element analyses. The analytical field solutions allow the prediction of the thrust force, the winding emf, and the self- and mutual-winding inductances in closed forms. These facilitate the characterization of tubular machine topologies and provide a basis for comparative studies, design optimization, and machine dynamic modeling. Some practical issues, such as the effects of slotting and fringing, have also been accounted for and validated by measurements.

Index Terms—Electromagnetic analysis, electromagnetic fields, linear motors, magnetic fields, permanent magnet machines, permanent magnets.

I. INTRODUCTION

LINEAR electromagnetic machines, which can provide thrust force directly to a payload or generate power from applied thrusts, are being employed increasingly in applications ranging from transportation, manufacturing, and office automation to material processing, health care, and generation systems. Particular examples include stirling cycle cryogenic coolers and generators [1], [2] and artificial heart devices [3]. Such direct linear electro-mechanical energy conversion devices offer numerous advantages over their rotary-to-linear counterparts, notably the absence of mechanical gears and transmission systems, which results in a higher dynamic performance and improved reliability. Among various linear machine configurations, tubular machines with permanent magnet excitation have a number of distinctive features [4], such as a high force density and excellent servo characteristics, which make them an attractive candidate for applications in which dynamic performance and reliability are crucial [2], [3].

In order to facilitate the design optimization and accurate dynamic modeling of linear permanent magnet machines, a variety of techniques have been employed to predict the magnetic field distribution [5], the most common approach being to use a lumped equivalent circuit [1], [6]. However, while this allows the relationship between critical design parameters and

machine performance to be established analytically, it suffers from problems associated with model inaccuracy, particularly when flux leakage is significant and the flux paths are complex. With the availability of powerful software tools, numerical analysis of the field distribution and evaluation of performance [7]–[8] has also become common practice. However, while numerical techniques, such as finite element analysis, provide an accurate means of determining the field distribution, with due account of saturation etc., they remain time-consuming and do not provide as much insight as analytical solutions into the influence of the design parameters on the machine behavior. To overcome the aforementioned problems, a two-dimensional (2-D) analytical solution for the magnetic field distribution was established in the rectangular coordinate system for a single-sided, flat linear permanent magnet motor, using the magnetic charge image technique [9]. Analytical treatments based on the magnetic vector potential were also adopted in [10] and [11] to predict the 2-D flux distribution in such machines. However, analytical solutions for the field in tubular linear permanent magnet machines, which would be extremely useful for their design and performance optimization, have not been available in literature, to date.

This paper attempts to provide a unified framework for the analysis and design of the class of tubular linear permanent magnet machines which embraces the topologies shown in Fig. 1. For this purpose, the magnetic field distribution is established using an analytical technique formulated in the cylindrical coordinate system, and the results are verified by finite element analyses. The analytical solutions allow the prediction of the thrust force, the back emf, and the winding inductances in closed forms. In turn, these facilitate the characterization of the machines and provide a basis for comparative studies, design optimization, system dynamic modeling and simulations, and servo-control development.

II. FIELD DISTRIBUTION DUE TO PERMANENT MAGNET SOURCE

As highlighted in Fig. 1, there are numerous variants of tubular linear permanent magnet machines. Fig. 1(a) and (b) shows internal and external magnet topologies with radially magnetized magnets, respectively, both of which could be either moving magnet or moving armature [1], [12]. Fig. 1(c) shows a topology with axially magnetized magnets separated by iron pole pieces [13], while Fig. 1(d) employs a multi-pole Halbach magnetization [14]. In all these topologies, the armature could be either air- or iron-cored, in which case it could be either slotless or slotted, while one member may

Manuscript received January 15, 1998; revised January 15, 1998. This work was supported by EPSRC for the provision of a ROPA award.

J. Wang is with the School of Electrical and Manufacturing Engineering, University of East London, Dagenham, Essex, RM8 2AS U.K.

G. W. Jewell and D. Howe are with the Department of Electronic and Electrical Engineering, University of Sheffield, Sheffield, S1 3JD U.K.

Publisher Item Identifier S 0018-9464(99)03870-4.

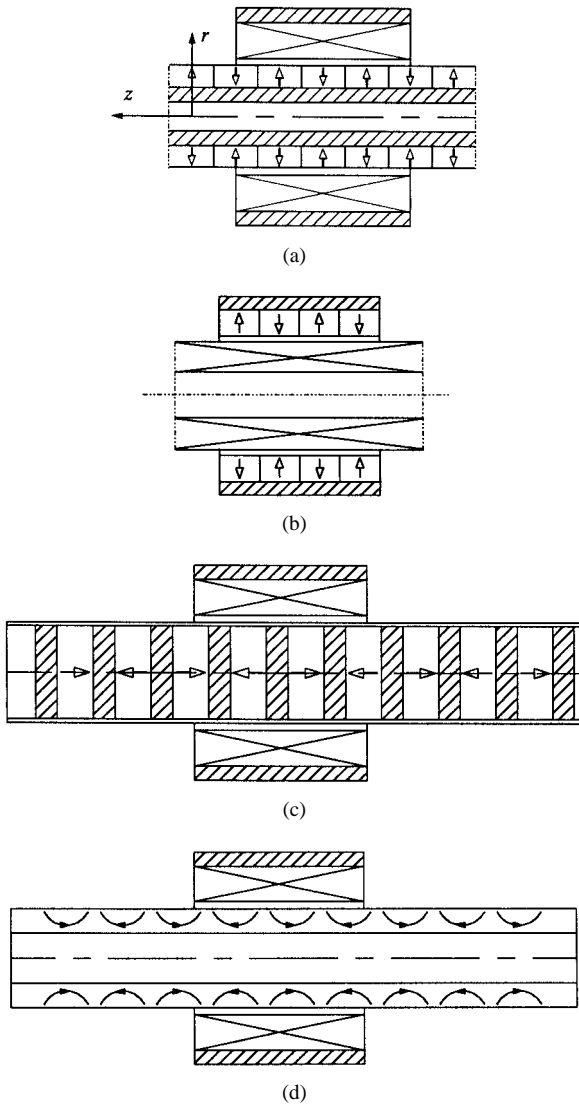


Fig. 1. Typical tubular linear permanent magnet machine topologies: (a) radial magnetization, internal magnet topology [1], (b) radial magnetization, external magnet topology [12], (c) axial magnetization, internal magnet topology [13], and (d) Halbach magnetization, internal magnet topology [15].

be longer than the other dependent on the required stroke. Generally, the preferred topology depends on the application. Slotted iron-cored topologies usually have a higher force density, but may also produce an undesirable destabilizing tooth ripple cogging force and have the highest eddy current losses in the magnets and the iron, especially when operating at high speed. Slotless armature topologies, on the other hand, eliminate the tooth ripple cogging effect, and thereby improve the dynamic performance and servo characteristic at the expense of a reduction in specific force capability, although the cogging force associated with the finite length of the iron-cored armature may still be significant if it is not designed accordingly [13].

In order to establish analytical solutions for the magnetic field distribution in the foregoing machine topologies, the following assumptions are made:

- 1) The axial length of the machines is infinite so that the field distribution is axially-symmetric and periodic in

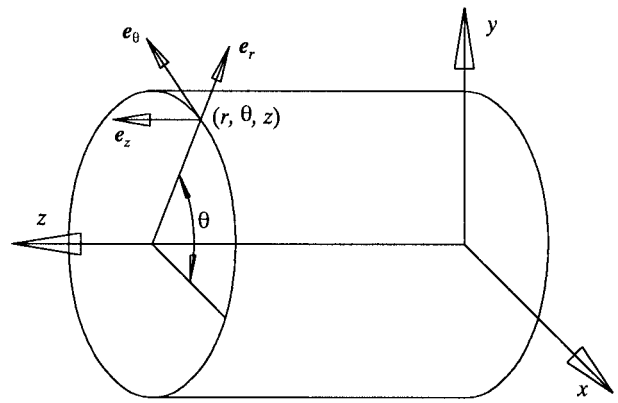


Fig. 2. Cylindrical coordinate system.

the z direction. However, fringing effects associated with the finite length of the armature will be considered in Section III.

- 2) The armature is slotless, and the permeability of the iron is infinite. However, slotting effects, if present, can be taken into account by introducing a Carter coefficient [15], as will be shown in Section III.

Consequently, the magnetic field analysis is confined to two regions, viz., the airspace/winding region in which the permeability is μ_0 , and the permanent magnet region in which the permeability is $\mu_0\mu_r$. Therefore

$$\mathbf{B} = \begin{cases} \mu_0\mathbf{H}, & \text{in the airspace/winding} \\ \mu_0\mu_r\mathbf{H} + \mu_0\mathbf{M}, & \text{in the magnets} \end{cases} \quad (1)$$

where μ_r is the relative recoil permeability of the magnets and \mathbf{M} is the remanent magnetization. For a permanent magnet having a linear demagnetization characteristic, μ_r is constant and the magnetization \mathbf{M} is related to the remanence \mathbf{B}_{rem} by $\mathbf{M} = \mathbf{B}_{rem}/\mu_0$. It is convenient to formulate the field distribution in terms of a magnetic vector potential \mathbf{A} defined as $\mathbf{B} = \nabla \times \mathbf{A}$, and the cylindrical coordinate system shown in Fig. 2. The governing field equations, in terms of the Coulomb gauge, $\nabla \cdot \mathbf{A} = 0$, are

$$\begin{cases} \nabla^2 \mathbf{A}_I = 0, & \text{in the airspace/winding} \\ \nabla^2 \mathbf{A}_{II} = -\mu_0 \nabla \times \mathbf{M}, & \text{in the magnets.} \end{cases} \quad (2)$$

Since the field is axially symmetric, \mathbf{A} only has the component A_θ , which is independent of θ . This leads to (3) shown at the bottom of the next page. In the cylindrical coordinate system, the magnetization \mathbf{M} is given by

$$\mathbf{M} = M_r \mathbf{e}_r + M_z \mathbf{e}_z \quad (4)$$

where M_r and M_z denote the components of \mathbf{M} in the r and z directions, respectively. The flux density components are deduced from A_θ by

$$B_z = \frac{1}{r} \frac{\partial}{\partial r}(rA_\theta); \quad B_r = -\frac{\partial A_\theta}{\partial z}.$$

The form of the solutions to (3) depends on the machine topology, each of which will be considered separately as follows.

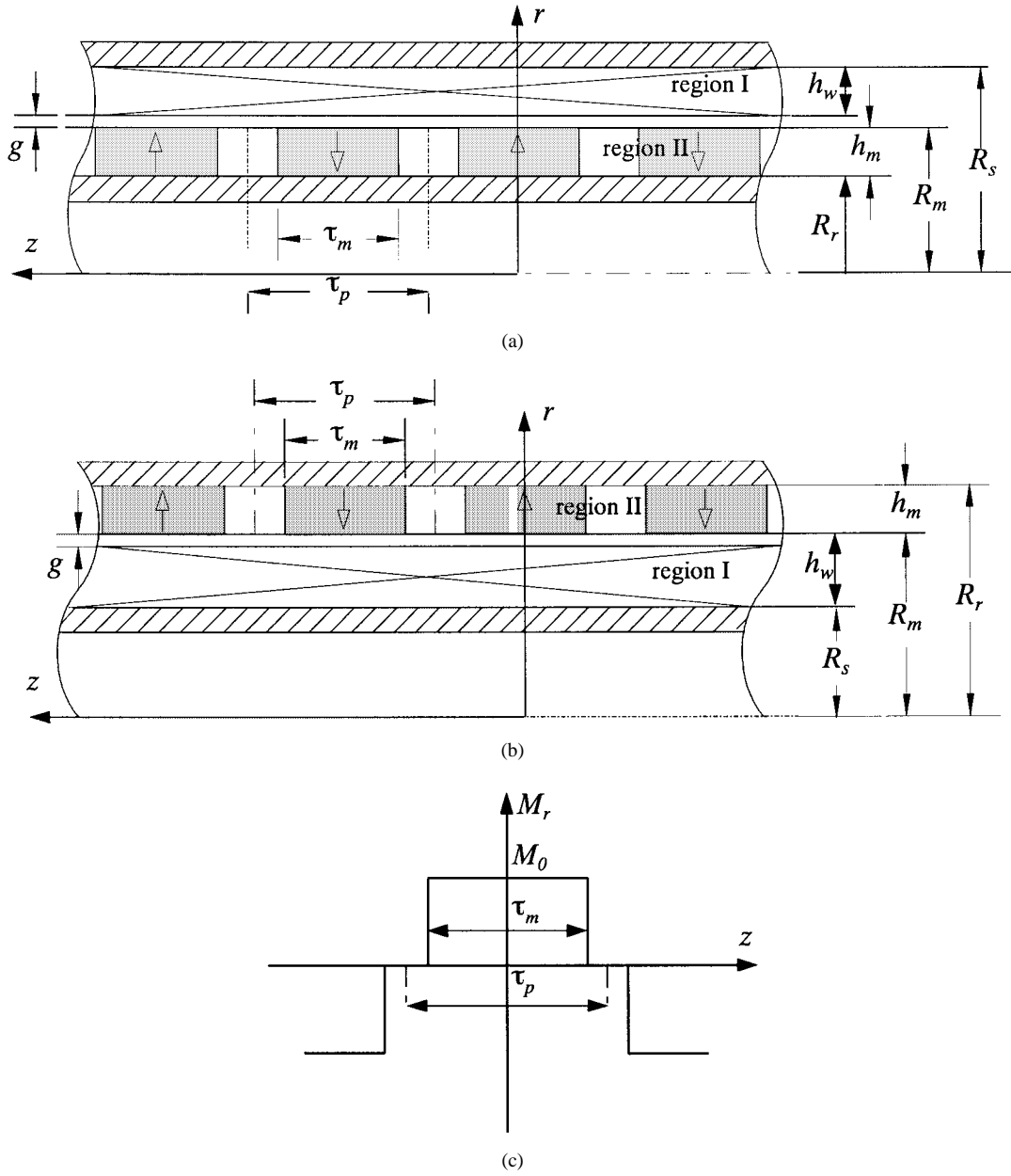


Fig. 3. Field regions of radially magnetized machine topologies: (a) internal magnet topology, (b) external magnet topology, and (c) magnetization distribution.

A. Radial Magnetization Machine Topologies

Fig. 3(a) and (b) shows simplified models of the internal and external radially magnetized machine topologies, in which $M_z = 0$ and M_r have the distribution shown in Fig. 3(c), which may be expanded into a Fourier series of the form

$$M_r = \sum_{n=1,2,\dots}^{\infty} 4(B_{rem}/\mu_0) \frac{\sin(2n-1)\frac{\pi}{2}\alpha_p}{(2n-1)\pi} \cos m_n z \quad (5)$$

where α_p is the ratio of magnet pole-length τ_m to pole-pitch τ_p , and $m_n = (2n-1)\pi/\tau_p$.

Combining (3)–(5) yields (6) (shown at the bottom of the next page) where $P_n = \frac{4}{\tau_p} B_{rem} \sin(2n-1)\frac{\pi}{2}\alpha_p$. The boundary conditions to be satisfied by the solution to (6) are:

$$\begin{aligned} B_{Iz}|_{r=R_s} &= 0; & B_{IIz}|_{r=R_r} &= 0 \\ B_{Iz}|_{r=R_m} &= B_{IIz}|_{r=R_m}; & H_{Iz}|_{r=R_m} &= H_{IIz}|_{r=R_m} \end{aligned} \quad (7)$$

$$\begin{cases} \frac{\partial}{\partial z} \left(\frac{1}{r} \frac{\partial}{\partial z} (r A_{I\theta}) \right) + \frac{\partial}{\partial r} \left(\frac{1}{r} \frac{\partial}{\partial r} (r A_{I\theta}) \right) = 0 & \text{in the airspace/winding} \\ \frac{\partial}{\partial z} \left(\frac{1}{r} \frac{\partial}{\partial z} (r A_{II\theta}) \right) + \frac{\partial}{\partial r} \left(\frac{1}{r} \frac{\partial}{\partial r} (r A_{II\theta}) \right) = -\mu_0 \nabla \times \mathbf{M} & \text{in the magnets.} \end{cases} \quad (3)$$

where

$$\begin{aligned} R_m &= R_s - (g + h_w) & \text{and} & & R_r &= R_s - (g + h_w + h_m) \\ & & & & & \text{for internal magnet machines} \\ R_m &= R_r - h_m & \text{and} & & R_s &= R_r - (g + h_w + h_m) \\ & & & & & \text{for external magnet machines} \end{aligned}$$

g being the airgap length, h_w the winding thickness for a slotless armature, and h_m the radial thickness of the magnets. Solving (6) subject to the boundary conditions of (7) yields (8) and (9) shown at the bottom of the page, for the component flux density distributions, where $BI_0(\bullet)$, $BI_1(\bullet)$ are modified *Bessel* functions of the first kind; $BK_0(\bullet)$, $BK_1(\bullet)$ are modified *Bessel* functions of the second kind, of order zero and one, respectively; and $F_{An}(\bullet)$, $F_{Bn}(\bullet)$, a_{In} , b_{In} , a_{II_n} and b_{II_n} are defined in Appendix A.

B. Halbach Cylinder Machine Topology

By analogy with rotary machines [14], the radially magnetized magnets in Fig. 3 could be replaced by a z - r polarized, multipole Halbach magnets in which the magnetization \mathbf{M} is given by

$$\begin{aligned} \mathbf{M} &= M_0 \cos(pz)\mathbf{e}_r - M_0 \sin(pz)\mathbf{e}_z \\ & \text{for internal magnet machines} \\ \mathbf{M} &= M_0 \cos(pz)\mathbf{e}_r + M_0 \sin(pz)\mathbf{e}_z \\ & \text{for external magnet machines} \end{aligned}$$

where $p = \pi/\tau_p$. The governing field equations, in terms of A_θ , then become (10) as shown at the bottom of the page. The flux density distributions, which satisfy the boundary conditions of (7), are now given by

$$\begin{aligned} B_{Ir}(r, z) &= -[a_{Ip}BI_1(pr) + b_{Ip}BK_1(pr)] \cos(pz) \\ B_{Iz}(r, z) &= [a_{Ip}BI_0(pr) - b_{Ip}BK_0(pr)] \sin(pz) \end{aligned} \quad (11)$$

$$\begin{aligned} B_{IIr}(r, z) &= -\{[F_{Ap}(pr) + a_{IIp}]BI_1(pr) \\ & \quad + [-F_{Bp}(pr) + b_{IIp}]BK_1(pr)\} \cos(pz) \\ B_{IIz}(r, z) &= \{[F_{Ap}(pr) + a_{IIp}]BI_0(pr) \\ & \quad + [F_{Bp}(pr) + b_{IIp}]BK_0(pr)\} \sin(pz) \end{aligned} \quad (12)$$

where $F_{Ap}(\bullet)$, $F_{Bp}(\bullet)$, a_{Ip} , b_{Ip} , a_{IIp} , and b_{IIp} are given in Appendix B. As can be seen, the flux density components are sinusoidally distributed with respect to z .

It is well known that an r - θ polarized, air-cored Halbach cylinder, which has been proposed for use in rotary machines, has a self-shielding property [14]. It will be shown, however, that this is not the case for an r - z polarized cylinder which might be employed in linear machines. The governing magnetic field equations for the r - z polarized, air-cored Halbach cylinder shown in Fig. 4, are given by (13) as shown at the bottom of the next page. The corresponding flux density distributions which satisfy the interface conditions

$$\begin{aligned} B_{Iz}|_{r=R_r} &= B_{IIz}|_{r=R_r}; & H_{Iz}|_{r=R_r} &= H_{IIz}|_{r=R_r} \\ B_{IIz}|_{r=R_m} &= B_{IIIz}|_{r=R_m}; & H_{IIz}|_{r=R_m} &= H_{IIIz}|_{r=R_m} \end{aligned} \quad (14)$$

$$\begin{cases} \frac{\partial}{\partial z} \left(\frac{1}{r} \frac{\partial}{\partial z} (rA_{I\theta}) \right) + \frac{\partial}{\partial r} \left(\frac{1}{r} \frac{\partial}{\partial r} (rA_{I\theta}) \right) = 0 & \text{in the airspace/winding} \\ \frac{\partial}{\partial z} \left(\frac{1}{r} \frac{\partial}{\partial z} (rA_{II\theta}) \right) + \frac{\partial}{\partial r} \left(\frac{1}{r} \frac{\partial}{\partial r} (rA_{II\theta}) \right) = \sum_{n=1,2,\dots}^{\infty} P_n \sin m_n z & \text{in the magnets} \end{cases} \quad (6)$$

$$\begin{aligned} B_{Ir}(r, z) &= - \sum_{n=1,2,\dots}^{\infty} [a_{In}BI_1(m_n r) + b_{In}BK_1(m_n r)] \cos(m_n z) \\ B_{Iz}(r, z) &= \sum_{n=1,2,\dots}^{\infty} [a_{In}BI_0(m_n r) - b_{In}BK_0(m_n r)] \sin(m_n z) \\ B_{IIr}(r, z) &= - \sum_{n=1,2,\dots}^{\infty} \{ [F_{An}(m_n r) + a_{II_n}]BI_1(m_n r) \\ & \quad + [-F_{Bn}(m_n r) + b_{II_n}]BK_1(m_n r) \} \cos(m_n z) \\ B_{IIz}(r, z) &= - \sum_{n=1,2,\dots}^{\infty} \{ [F_{An}(m_n r) + a_{II_n}]BI_0(m_n r) \\ & \quad + [F_{Bn}(m_n r) - b_{II_n}]BK_0(m_n r) \} \sin(m_n z) \end{aligned} \quad (8)$$

$$\begin{aligned} B_{IIz}(r, z) &= - \sum_{n=1,2,\dots}^{\infty} \{ [F_{An}(m_n r) + a_{II_n}]BI_0(m_n r) \\ & \quad + [F_{Bn}(m_n r) - b_{II_n}]BK_0(m_n r) \} \sin(m_n z) \end{aligned} \quad (9)$$

$$\begin{cases} \frac{\partial}{\partial z} \left(\frac{1}{r} \frac{\partial}{\partial z} (rA_{I\theta}) \right) + \frac{\partial}{\partial r} \left(\frac{1}{r} \frac{\partial}{\partial r} (rA_{I\theta}) \right) = 0 & \text{in the airspace/winding} \\ \frac{\partial}{\partial z} \left(\frac{1}{r} \frac{\partial}{\partial z} (rA_{II\theta}) \right) + \frac{\partial}{\partial r} \left(\frac{1}{r} \frac{\partial}{\partial r} (rA_{II\theta}) \right) = pB_{rem} \sin pz & \text{in the magnets} \end{cases} \quad (10)$$

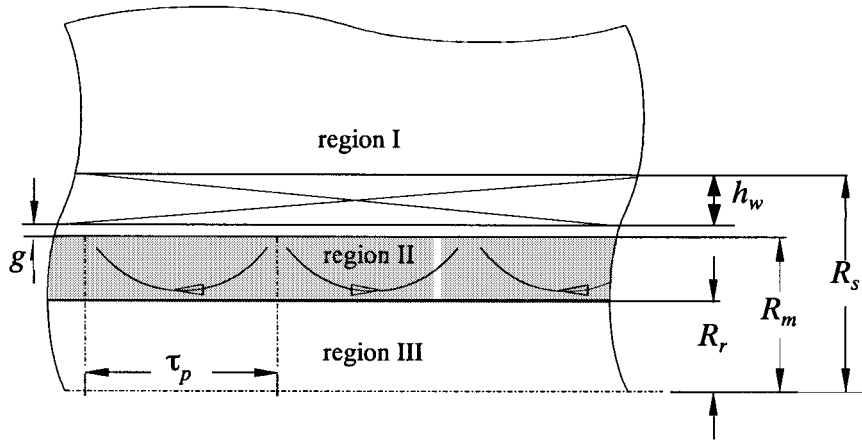


Fig. 4. Field regions of air-cored Halbach cylinder machine topology.

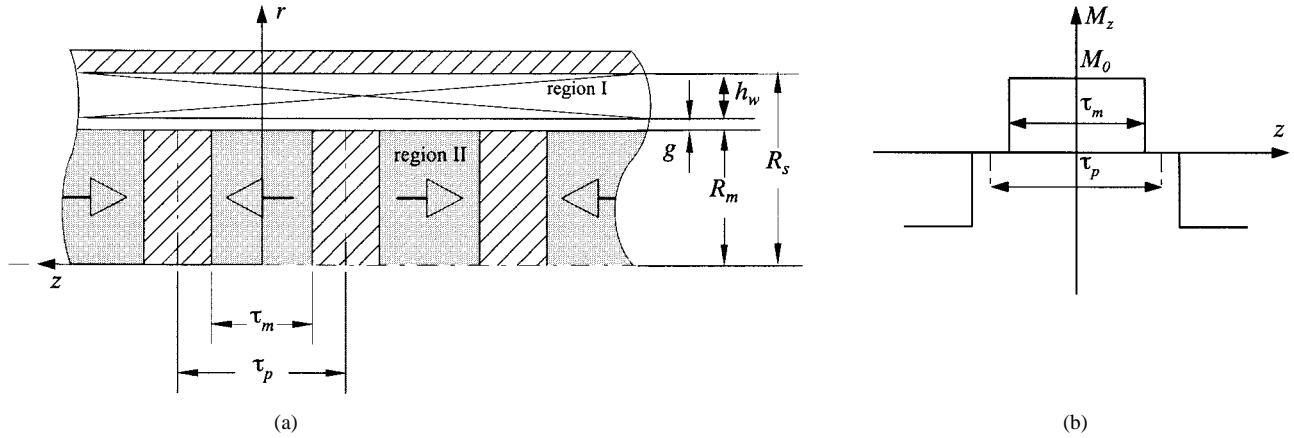


Fig. 5. Field regions of axially magnetized machine topology: (a) field regions and (b) magnetization distribution.

are

$$B_{I_r}(r, z) = -a'_{Ip}BK_1(pr) \cos(pz)$$

$$B_{I_z}(r, z) = -a'_{Ip}BK_0(pr) \sin(pz) \tag{15}$$

$$B_{II_r}(r, z) = - \left\{ [-F_{Ap}(pr) + a'_{Iip}]BI_1(pr) + [F_{Bp}(pr) + b'_{Iip}]BK_1(pr) \right\} \cos(pz)$$

$$B_{II_z}(r, z) = \left\{ [-F_{Ap}(pr) + a'_{Iip}]BI_0(pr) - [F_{Bp}(pr) + b'_{Iip}]BK_0(pr) \right\} \sin(pz) \tag{16}$$

$$B_{III_r}(r, z) = -a'_{IIIp}BI_1(pr) \cos(pz)$$

$$B_{III_z}(r, z) = a'_{IIIp}BI_0(pr) \sin(pz) \tag{17}$$

where a'_{Ip} , a'_{Iip} , b'_{Iip} , and a'_{IIIp} are given in Appendix C. Since these coefficients are not zero, it follows that the magnetic

field due to the Halbach cylinder has components in all three regions, implying that the cylinder does not exhibit a self-shielding flux pattern.

C. Axial Magnetization Machine Topology

Fig. 5(a) shows the field regions of an axially magnetized machine topology, in which the magnets are disposed with alternating polarity in the z direction and separated by infinitely permeable iron pole pieces. The magnetization vector is, therefore, given by

$$\mathbf{M} = M_z \mathbf{e}_z. \tag{18}$$

The distribution of M_z is shown in Fig. 5(b), and may be expressed as the Fourier series

$$M_z = \sum_{n=1,2,\dots}^{\infty} 4(B_{rem}/\mu_0) \frac{\sin(2n-1)\frac{\pi}{2}\alpha_p}{(2n-1)\pi} \cos m_n z. \tag{19}$$

$$\begin{cases} \frac{\partial}{\partial z} \left(\frac{1}{r} \frac{\partial}{\partial z} (rA_{I,III\theta}) \right) + \frac{\partial}{\partial r} \left(\frac{1}{r} \frac{\partial}{\partial r} (rA_{I,III\theta}) \right) = 0 & \text{in region I and III} \\ \frac{\partial}{\partial z} \left(\frac{1}{r} \frac{\partial}{\partial z} (rA_{II\theta}) \right) + \frac{\partial}{\partial r} \left(\frac{1}{r} \frac{\partial}{\partial r} (rA_{II\theta}) \right) = pB_{rem} \sin pz & \text{in the magnet} \end{cases} \tag{13}$$

TABLE I
PARAMETERS OF SLOTLESS TUBULAR LINEAR PERMANENT MAGNET MACHINES

Parameters	Machine topology		
	Radial magnetisation, internal magnet	Axial magnetisation, internal magnet	Air-cored Halbach cylinder internal magnet
R_s/R_m	2.0	2.0	2.0*
R_r/R_m	0.47	/	0.47
τ_m/τ_p	1.0	0.65	1.0

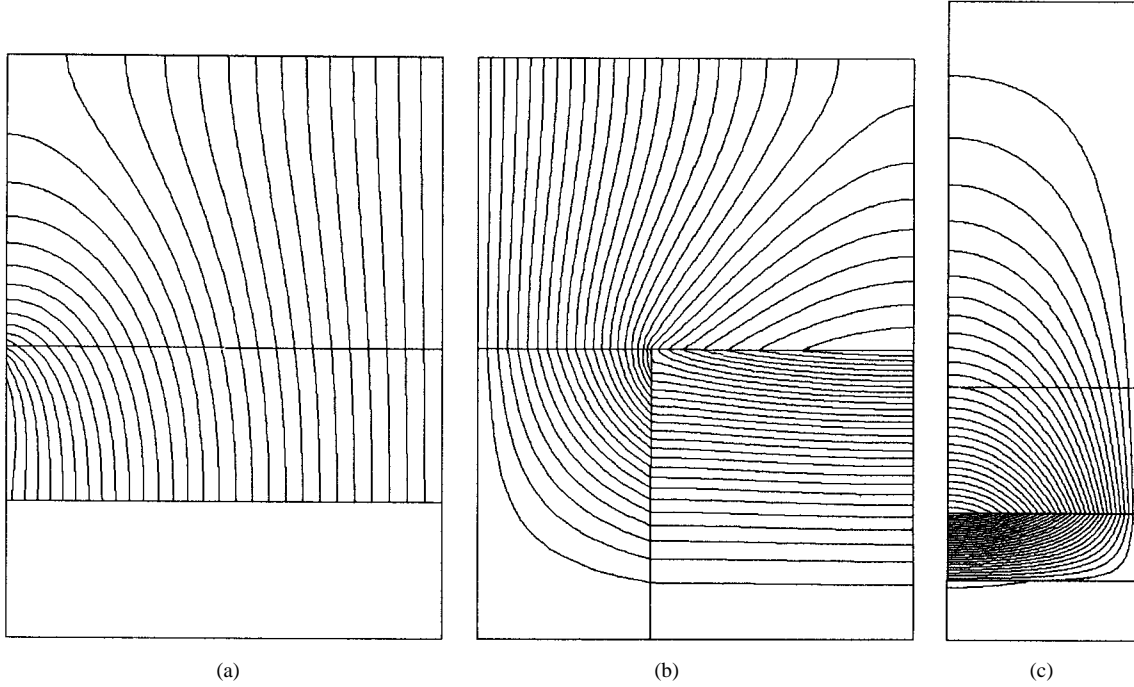


Fig. 6. Flux distributions of different internal magnet machine topologies: (a) radially magnetized, (b) axially magnetized, and (c) air-cored Halbach cylinder.

This leads to the governing field equations, in terms of A_θ , of the form shown at the bottom of the next page in (20). The boundary conditions to be satisfied by the solution to (20) are

$$\begin{aligned}
 B_{Iz}|_{r=R_s} &= 0; & B_{IIr}|_{r=0} &= 0 \\
 B_{IIr}|_{z=\pm\tau_m/2} &= 0; & B_{Iz}|_{\tau_m/2 \leq z \leq \tau/2} &= 0 \\
 B_{Ir}|_{-\tau_m/2 \leq z \leq \tau_m/2} &= B_{IIr}|_{-\tau_m/2 \leq z \leq \tau_m/2} \\
 H_{Iz}|_{-\tau_m/2 \leq z \leq \tau_m/2} &= H_{IIz}|_{-\tau_m/2 \leq z \leq \tau_m/2} \\
 \int_0^{R_m} 2\pi r B_{IIz} dr &= \int_{\tau_m/2}^{\tau/2} 2\pi R_m B_{Ir} dz. \quad (21)
 \end{aligned}$$

Solving (20) subject to the boundary conditions of (21) yields

$$\begin{aligned}
 B_{Ir}(r, z) &= \sum_{n=1,2,\dots}^{\infty} [a'_{In} B I_1(m_n r) + b'_{In} B K_1(m_n r)] \sin(m_n z) \\
 B_{Iz}(r, z) &= \sum_{n=1,2,\dots}^{\infty} [a'_{In} B I_0(m_n r) - b'_{In} B K_0(m_n r)] \cos(m_n z) \quad (22)
 \end{aligned}$$

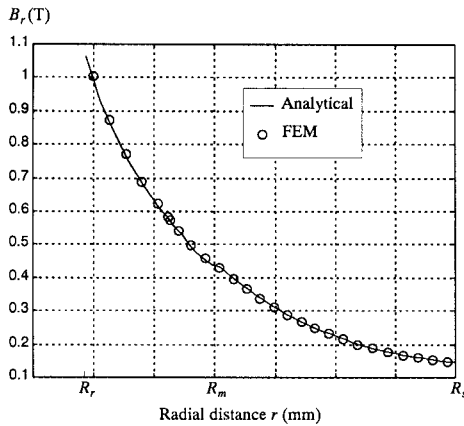
$$\begin{aligned}
 B_{IIr}(r, z) &= \sum_{j=1,2,\dots}^{\infty} \{a'_{IIj} B I_1(q_j r)\} \sin(q_j z) \\
 B_{IIz}(r, z) &= \sum_{j=1,2,\dots}^{\infty} \{a'_{IIj} B I_0(q_j r)\} \cos(q_j z) + B_0 \quad (23)
 \end{aligned}$$

where $q_j = 2\pi j/\tau_m$, and a'_{In} , b'_{In} , a'_{IIj} , b'_{IIj} , and B_0 are defined in Appendix D.

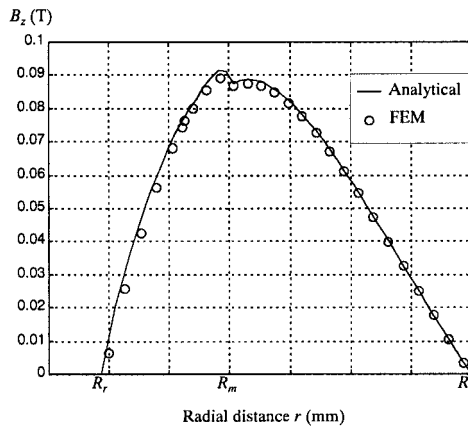
D. Comparison with Finite Element Calculations

The main design parameters of three different topologies of slotless tubular linear machines, for which analytical field solutions have been obtained, are given in Table I. The magnets are sintered NdFeB, with $B_{rem} = 1.2$ (T) and $\mu_r = 1.05$. The analytical field distributions have been validated by finite element calculations of the radial and axial variations of flux density in both the magnets and airgap/winding regions.

The finite element solutions were obtained by applying a periodic boundary condition at the axial boundaries and imposing the natural Neuman boundary condition at the surfaces of the stator and armature iron cores. Fig. 6 shows the resulting flux distributions for different machine topologies. Fig. 7



(a)



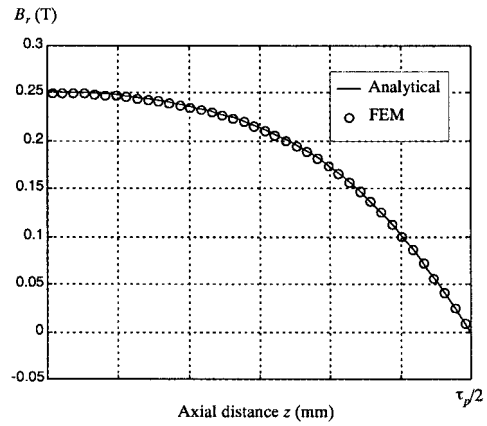
(b)

Fig. 7. Comparison of flux density components as functions of r at $z = \tau_p/4$. Radially magnetized, internal magnet machine topology: (a) radial component and (b) axial component.

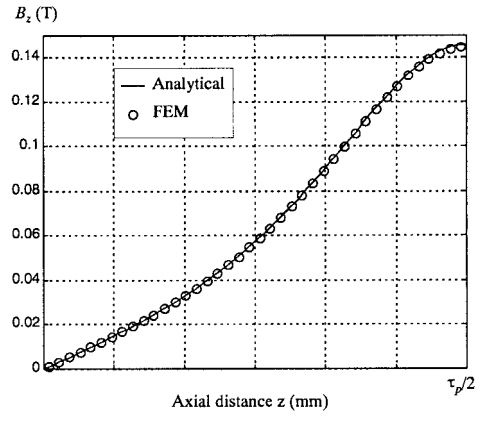
compares flux density components in the radially magnetized, internal magnet machine topology as functions of radius r at a constant axial position, while Fig. 8 compares the flux density components as functions of axial position z at a constant radius. Similar comparisons are presented in Figs. 9 and 10 for the axially magnetized machine topology. It will be seen that, in both cases, the analytical solutions agree extremely well with the finite element results. Figs. 11 and 12 show comparisons for the air-cored Halbach cylinder machine, for which it will be noted that the flux density inside the bore of the cylinder ($r < R_r$) is not zero, although it has a relatively small magnitude, as was mentioned earlier. It can also be observed that the flux density in the airgap/winding region is sinusoidally distributed with respect to the axial coordinate z .

III. FORCE AND EMF PREDICTION

Without loss of generality, the emf and force can be calculated for both internal and external magnet machine



(a)



(b)

Fig. 8. Comparison of flux density components as functions of z at $r = (R_m + R_s)/2$. Radially magnetized, internal magnet machine topology: (a) radial component and (b) axial component.

topologies. However, the following derivations are undertaken for internal magnet machine topologies. Nevertheless, the analysis can be readily modified to cater for external magnet machine topologies.

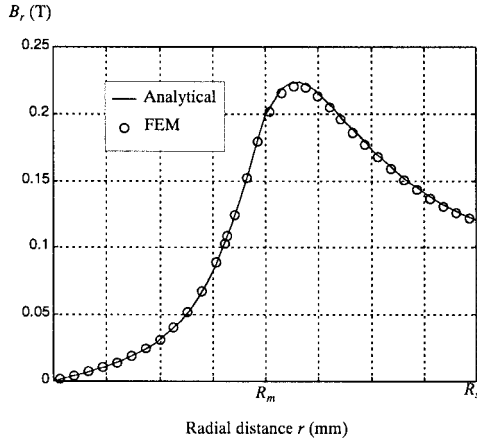
A. Slotless Armature

The thrust force exerted on the armature, resulting from the interaction between the winding current and the permanent magnet field, is given by

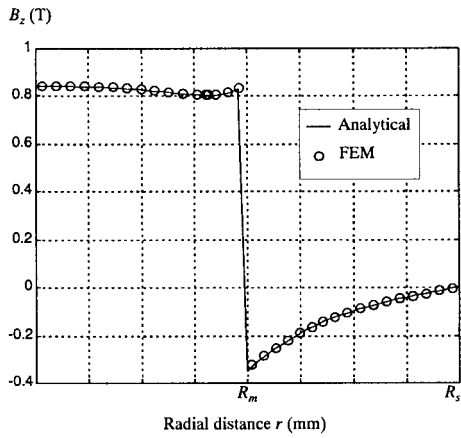
$$\mathbf{F}_w = \int_V (\mathbf{J} \times \mathbf{B}) dV \quad (24)$$

where \mathbf{J} denotes the current density vector in the winding region V . Assuming that each winding coil on the armature comprises a number of circular turns, and occupies an area bounded by $r_1 = R_i$, $r_2 = R_s$, $z_1 = z - \tau_w/2$, and $z_2 = z + \tau_w/2$, as shown in Fig. 12, where τ_w is the coil

$$\begin{cases} \frac{\partial}{\partial z} \left(\frac{1}{r} \frac{\partial}{\partial z} (r A_{I\theta}) \right) + \frac{\partial}{\partial r} \left(\frac{1}{r} \frac{\partial}{\partial r} (r A_{I\theta}) \right) = 0 & \text{in the airspace/winding} \\ \frac{\partial}{\partial z} \left(\frac{1}{r} \frac{\partial}{\partial z} (r A_{II\theta}) \right) + \frac{\partial}{\partial r} \left(\frac{1}{r} \frac{\partial}{\partial r} (r A_{II\theta}) \right) = 0 & \text{in the magnets} \end{cases} \quad (20)$$



(a)



(b)

Fig. 9. Comparison of flux density components as functions of r at $z = \tau_p/4$. Axially magnetized, internal magnet machine topology: (a) radial component and (b) axial component.

axial width, the total thrust force exerted on the coil may be obtained from the following integration:

$$F_w = - \int_{z-\tau_w/2}^{z+\tau_w/2} \int_{R_i}^{R_s} 2\pi r J B_{lr}(r, z) dr dz$$

which may be written as

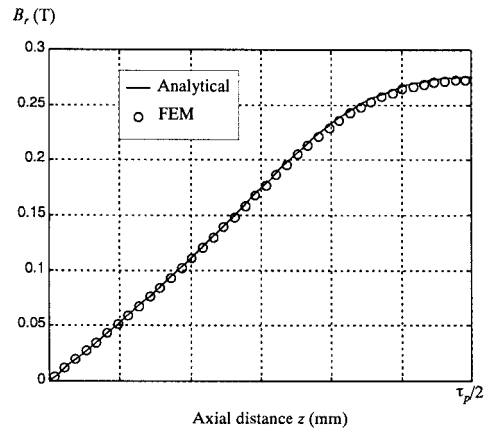
$$F_w = \sum_{n=1,2,\dots}^{\infty} F_n \cos m_n z \quad (25)$$

where R_i is the radius of the armature bore. For the radially magnetized machine topology, F_n is given by

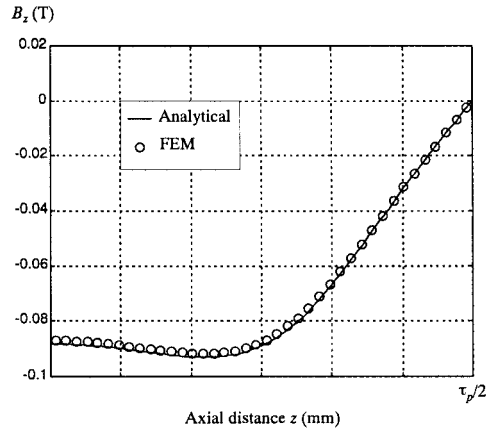
$$F_n = 2\pi\tau_w J K_{dn} \int_{R_i}^{R_s} r [a_{ln} B I_1(m_n r) + b_{ln} B K_1(m_n r)] dr. \quad (26)$$

$K_{dn} = \sin(m_n \tau_w/2)/(m_n \tau_w/2)$ is defined as the winding distribution factor of the $(2n - 1)$ th harmonic. Therefore, the total force F_{wp} exerted on a phase winding comprising a number of series connected coils, each displaced by a winding pitch τ_{wp} and carrying a current i , is obtained as

$$F_{wp} = \left(\sum_{n=1,2,\dots}^{\infty} K_{Tn} \sin m_n \left(z - \frac{\tau_{wp}}{2} \right) \right) i \quad (27)$$



(a)



(b)

Fig. 10. Comparison of flux density components as functions of z at $r = (R_m + R_s)/2$. Axially magnetized, internal magnet machine topology: (a) radial component and (b) axial component.

where K_{Tn} is defined as the torque constant of the $(2n - 1)$ th harmonic, and is given by

$$K_{Tn} = - \frac{2\pi K_{dpn} N_{wp}}{(R_s - R_i)} \int_{R_i}^{R_s} r [a_{ln} B I_1(m_n r) + b_{ln} B K_1(m_n r)] dr. \quad (28)$$

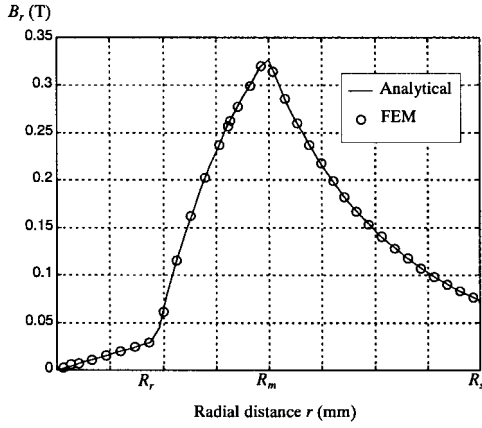
$K_{dpn} = K_{pm} K_{dn}$ is the winding factor of the $(2n - 1)$ th harmonic, $K_{pm} = \sin(m_n \tau_{wp}/2)$ being the winding pitch factor, K_{dn} the distribution factor, and N_{wp} the number of series turns per phase. For a linear machine employing an r - z magnetized Halbach cylinder, (27) and (28) can be simplified as

$$F_{wp} = [K_{Tp} \sin p(z - \tau_{wp}/2)] i \quad (29)$$

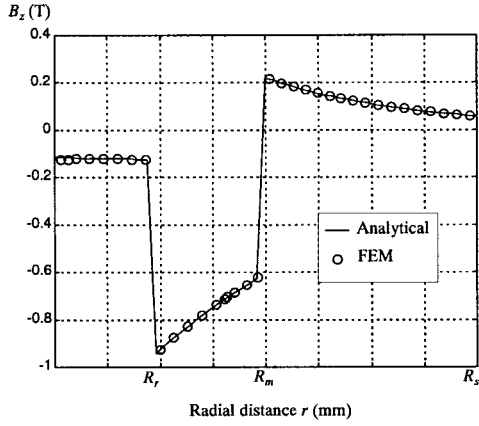
and

$$K_{Tp} = - \frac{2\pi K_{dp} N_{wp}}{(R_s - R_i)} \int_{R_i}^{R_s} r [a_{lp} B I_1(pr) + b_{lp} B K_1(pr)] dr. \quad (30)$$

For axially magnetized machine topologies, the force exerted on a phase winding can be similarly derived from the integra-



(a)



(b)

Fig. 11. Comparison of flux density components as functions of r at $z = \tau_p/4$. Air-cored Halbach cylinder, internal magnet machine topology: (a) radial component and (b) axial component.

tion procedure. Thus

$$F_{wp} = \left(\sum_{n=1,2,\dots}^{\infty} K_{Tn} \cos m_n \left(z - \frac{\tau_{wp}}{2} \right) \right) i \quad (31)$$

where K_{Tn} is given by

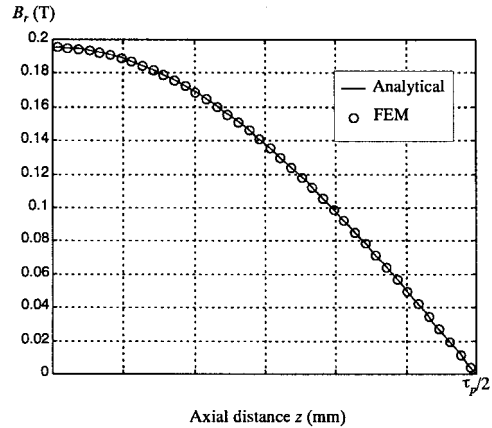
$$K_{Tn} = -\frac{2\pi K_{dpm} N_{wp}}{(R_s - R_i)} \int_{R_i}^{R_s} r [a'_{In} B I_1(m_n r) + b'_{In} B K_1(m_n r)] dr \quad (32)$$

With reference to Fig. 12, the coil flux-linkage for radially magnetized machine topologies can be obtained by the following integration:

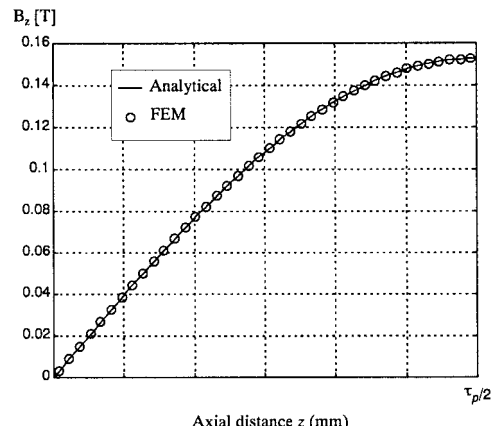
$$\psi_w = \int_{z-\tau_w/2}^{z+\tau_w/2} \int_{R_i}^{R_s} 2\pi r A_{I\theta}(r, z) dr dz = \sum_{n=1,2,\dots}^{\infty} \Phi_n \sin m_n z \quad (33)$$

where

$$\Phi_n = \frac{2\pi\tau_w}{m_n} K_{dn} \int_{R_i}^{R_s} r [a_{In} B I_1(m_n r) + b_{In} B K_1(m_n r)] dr. \quad (34)$$



(a)



(b)

Fig. 12. Comparison of flux density components as functions of z at $r = (R_m + R_s)/2$. Air-cored Halbach cylinder, internal magnet machine topology: (a) radial component and (b) axial component.

The total flux-linkage of a distributed multi-coil phase winding is, therefore, given by

$$\psi_{wp} = \sum_{n=1,2,\dots}^{\infty} \Phi_{np} \cos m_n \left(z - \frac{\tau_{wp}}{2} \right) \quad (35)$$

and

$$\Phi_{np} = \frac{2\pi K_{dpm} N_{wp}}{m_n (R_s - R_i)} \int_{R_i}^{R_s} r [a_{In} B I_1(m_n r) + b_{In} B K_1(m_n r)] dr. \quad (36)$$

Hence, the induced emf per phase is obtained as

$$e_{wp} = -\frac{d\psi_{wp}}{dt} = \left(-\sum_{n=1,2,\dots}^{\infty} K_{En} \sin m_n \left(z - \frac{\tau_{wp}}{2} \right) \right) v \quad (37)$$

where v is the linear velocity, and K_{En} is analogously defined as the back-emf constant of the $(2n - 1)$ th harmonic and is given by

$$K_{En} = -\frac{2\pi K_{dpm} N_{wp}}{(R_s - R_i)} \int_{R_i}^{R_s} r [a_{In} B I_1(m_n r) + b_{In} B K_1(m_n r)] dr. \quad (38)$$

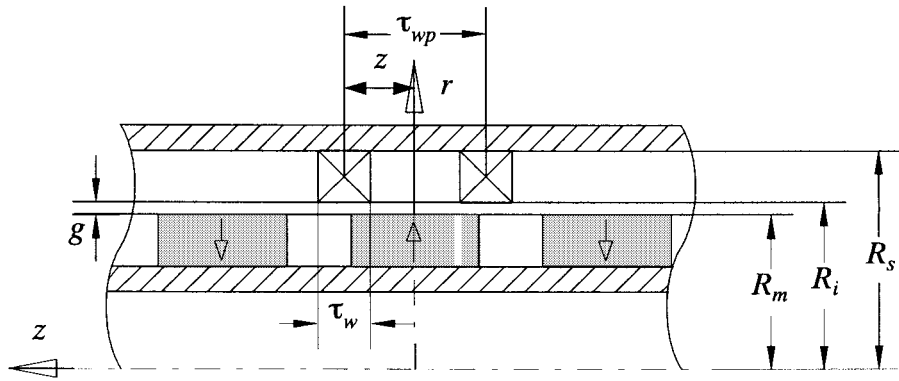


Fig. 13. Winding distribution.

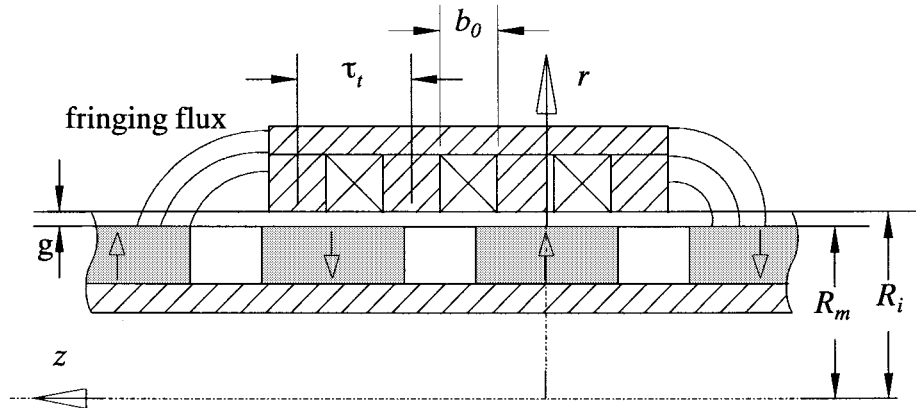


Fig. 14. Slotted armature and fringing effect.

As can be seen, K_{En} and K_{Tn} are identical, as in rotary brushed and brushless permanent magnet machines. Consequently, K_{En} for Halbach cylinder and axially magnetized machine topologies is given in (30) and (32), respectively.

B. Slotted, Finite Length Armature

If the armature is slotted and has a finite length, as shown in Fig. 14 for a radially magnetized, internal magnet machine topology, the effect of the slot openings may be accounted for by introducing a Carter coefficient K_c given by [15]

$$K_C = \frac{\tau_t}{\tau_t - \gamma g'} \quad (39)$$

where τ_t is the armature slot pitch, $g' = g + h_m/\mu_r$, and the slotting factor γ is given by

$$\gamma = \frac{4}{\pi} \left\{ \frac{b_0}{2g'} \tan^{-1} \left(\frac{b_0}{2g'} \right) - \ln \sqrt{1 + \left(\frac{b_0}{2g'} \right)^2} \right\} \quad (40)$$

where b_0 is the width of the armature slot openings. Therefore, the effective airgap g_e and the equivalent armature bore radius R_{ie} are given, respectively, by

$$g_e = g + (K_c - 1)g' \quad (41)$$

$$R_{ie} = \begin{cases} R_m + g_e, & \text{for internal magnet topologies} \\ R_m - g_e, & \text{for internal magnet topologies.} \end{cases} \quad (42)$$

The distribution of the radial component of flux density at the armature bore $B_a(z)$ is given by

$$B_a(z)|_{r=R_{ie}} = B_{lr}(z, R_{ie}) \quad (43)$$

where B_{lr} is the radial flux density calculated using the effective airgap g_e . Consequently, the force or emf constant of the $(2n - 1)$ th harmonic for the different slotted armature machine topologies is obtained as (44) shown at the bottom of the page. In all linear machines, there is fringing flux due to their finite length, and this is particularly significant in slotted machines with a small airgap. It results in a net increase in

$$\begin{aligned} K_{Tn} &= -2\pi K_{dpm} N_{wp} R_{ie} [a_{ln} B I_1(m_n R_{ie}) + b_{ln} B K_1(m_n R_{ie})] && \text{for radially magnetized} \\ &&& \text{machine topologies} \\ K_{Tp} &= -2\pi K_{dp} N_{wp} R_{ie} [a_{lp} B I_1(p R_{ie}) + b_{lp} B K_1(p R_{ie})] && \text{for Halbach cylinder} \\ &&& \text{machine topologies} \\ K_{Tn} &= 2\pi K_{dpm} N_{wp} R_{ie} [a'_{ln} B I_1(m_n R_{ie}) + b'_{ln} B K_1(m_n R_{ie})] && \text{for axially magnetized} \\ &&& \text{machine topologies} \end{aligned} \quad (44)$$

armature winding flux linkage, as is indicated in Fig. 14, in a similar manner to rotary permanent magnet machines with overhanging magnets. To account for fringing flux in rotary machines, an analytical model was developed [16], in 2-*d* rectangular coordinates, for predicting the flux linkage when the magnets face either a slotted or slotless infinitely permeable boundary, but neglecting the effect of radial flux focusing. A simpler model was established in [17] which assumed circular fringing flux paths, the fringing effect being accounted for by introducing a magnet overhang factor k_{mo} given by

$$k_{mo} = 1 + c \ln \left[1 + \frac{1}{c} \left(\frac{l_m}{l_a} - 1 \right) \right] \quad (45)$$

where l_a and l_m are the armature and magnet lengths, respectively, and c is given by

$$c = \frac{4h_m}{\pi\mu_r l_a} \left(\frac{A_g}{A_m} + \mu_r \frac{g}{h_m} \right) \quad (46)$$

where A_g and A_m are the cross-sectional areas of the airgap and the magnet, respectively. For cylindrical machines, curvature and flux focusing effects may be taken into account using the average cross-sectional areas given by:

$$A_g/A_m = (R_i + R_m)/(R_m + R_r). \quad (47)$$

It was shown in [17] that predictions of fringing flux by the use of (45) agree well with results obtained from the method in [16] as well as from 3-*d* finite element calculations. The magnet overhang factor has, therefore, been employed to account for fringing in slotted tubular linear machines. Thus, (44) is modified to (48) shown at the bottom of the page.

C. Validation

A two-phase tubular linear permanent magnet motor with a high specific force capability and dynamic bandwidth was recently developed [18]. It employs a radial magnetization, internal magnet topology, and a slotted armature. Fig. 15 compares the measured and predicted flux linkage of a phase winding having 202 turns, assuming a magnet overhang of two pole pitches in the prediction. As will be seen, the predicted flux linkage is essentially sinusoidal, the harmonic distortion being less than 0.5%, and agrees well with the measured waveform. From the motor design parameters, the predicted motor torque constant is 22.4 (Nm/A), which again compares favorably with the measured value of 24 (Nm/A), the error between the two being less than 7.0%, and attributable to an axial inhomogeneity in the extruded, radially anisotropic NdFeB magnets.

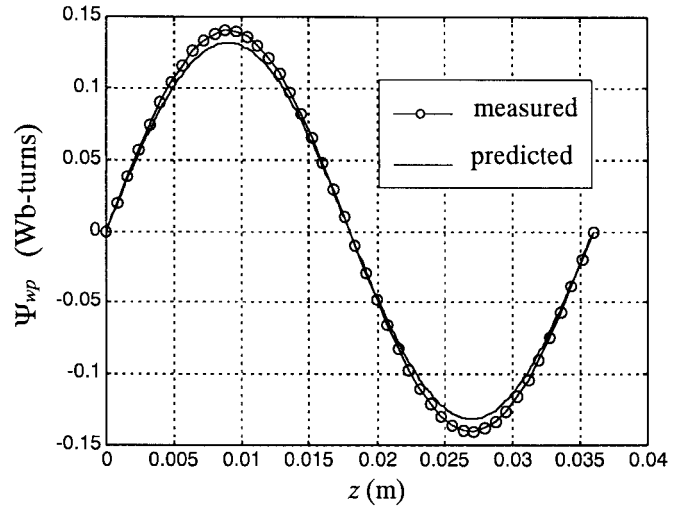


Fig. 15. Measured and predicted flux-linkage waveform of a phase winding.

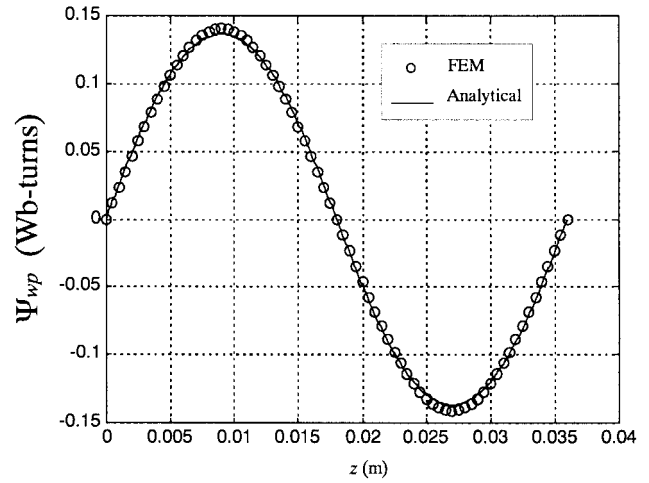


Fig. 16. Comparison of flux-linkage waveform of a phase winding.

Fig. 16 compares the analytical and finite element calculated flux linkage of a phase winding of a slotless version of the motor having 496 turns per phase. Since the effective airgap of the slotless motor is considerably larger than for the slotted motor, fringing effects have been neglected in the analytical calculation. However, the finite element calculation accounts for saturation and end effects associated with the finite armature length. As will be seen, the predicted flux-linkage waveforms agree well, the maximum error being less than 2%, indicating that fringing effects are negligible for this particular slotless machine.

$$\begin{aligned}
 K_{Tn} &= -2\pi k_{mo} K_{dpm} N_{wp} R_{ie} [a_{In} B I_1(m_n R_{ie}) + b_{In} B K_1(m_n R_{ie})] && \text{for radially magnetised} \\
 & && \text{machine topologies} \\
 K_{Tp} &= -2\pi k_{mo} K_{dp} N_{wp} R_{ie} [a_{Ip} B I_1(p R_{ie}) + b_{Ip} B K_1(p R_{ie})] && \text{for Halbach cylinder} \\
 & && \text{machine topologies} \\
 K_{Tn} &= 2\pi k_{mo} K_{dpm} N_{wp} R_{ie} [a'_{In} B I_1(m_n R_{ie}) + b'_{In} B K_1(m_n R_{ie})] && \text{for axially magnetised} \\
 & && \text{machine topologies}
 \end{aligned} \quad (48)$$

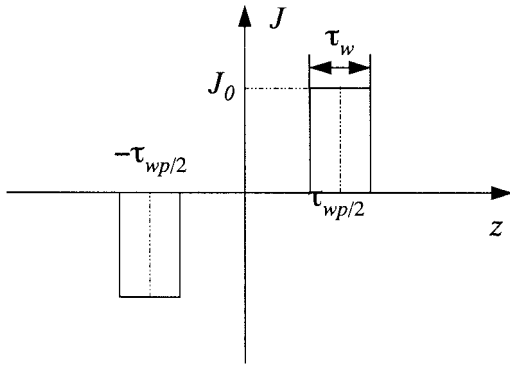


Fig. 17. Current distribution of a phase winding.

IV. ARMATURE REACTION FIELD AND INDUCTANCE

Assuming that the armature is slotless with a coil spread τ_w , and a winding pitch τ_{wp} , as shown in Fig. 12, the current distribution of a phase winding, as shown in Fig. 17, may be expanded into a Fourier series, viz

$$J(z) = \sum_{n=1,2,\dots}^{\infty} J_n \sin m_n z \quad (49)$$

where J_n is given by

$$J_n = \frac{4J_0}{\pi(2n-1)} \sin \frac{(2n-1)\tau_{wp}}{2\tau_p} \sin \frac{(2n-1)\tau_w}{2\tau_p}. \quad (50)$$

The armature reaction field equations, in terms of A_θ , are therefore given by (51) shown at the bottom of the page. The boundary conditions to be satisfied by (51) are

$$\begin{aligned} B_{\Pi z}|_{r=R_r} &= 0; & B_{\Pi z}|_{r=R_s} &= 0 \\ B_{\Pi z}|_{r=R_i} &= B_{\Pi z}|_{r=R_o}; & H_{\Pi z}|_{r=R_i} &= H_{\Pi z}|_{r=R_o} \end{aligned} \quad (52)$$

where R_i is the inner or outer radius of the armature for internal or external magnet topologies, respectively, and is given by

$$R_i = \begin{cases} R_m + g, & \text{for internal magnet topologies} \\ R_m - g, & \text{for external magnet topologies.} \end{cases} \quad (53)$$

Solving (51) by satisfying the boundary conditions of (52) and assuming $\mu_r = 1.0$, for simplicity, yields the following expressions for the flux density components:

$$\begin{aligned} B_{\Pi r}(r, z) &= - \sum_{n=1,2,\dots}^{\infty} \{ [F_{Aan}(m_n r) + a_{\text{Ian}}] BI_1(m_n r) \\ &\quad + [-F_{Ban}(m_n r) + b_{\text{Ian}}] BK_1(m_n r) \} \cos(m_n z) \\ B_{\Pi z}(r, z) &= \sum_{n=1,2,\dots}^{\infty} \{ [F_{Aan}(m_n r) + a_{\text{Ian}}] BI_0(m_n r) \\ &\quad + [F_{Ban}(m_n r) - b_{\text{Ian}}] BK_0(m_n r) \} \sin(m_n z) \end{aligned} \quad (54)$$

$$\begin{aligned} B_{\Pi r}(r, z) &= - \sum_{n=1,2,\dots}^{\infty} [a_{\text{IIan}} BI_1(m_n r) \\ &\quad + b_{\text{IIan}} BK_1(m_n r)] \cos(m_n z) \\ B_{\Pi z}(r, z) &= \sum_{n=1,2,\dots}^{\infty} [a_{\text{IIan}} BI_0(m_n r) \\ &\quad - b_{\text{IIan}} BK_0(m_n r)] \sin(m_n z) \end{aligned} \quad (55)$$

where $F_{Aan}(\bullet)$, $F_{Ban}(\bullet)$, a_{Ian} , b_{Ian} , a_{IIan} , and b_{IIan} are given in Appendix E. Equation (55) can be used to determine the extent, if any, of partial irreversible demagnetization of the magnets under various operation conditions. Similarly, the flux linkage of a phase winding having N_p pole pairs due to its own armature reaction field may be obtained by integration, and is given by

$$\psi_{wap} = \sum_{n=1,2,\dots}^{\infty} \Phi_{apn} \quad (56)$$

where

$$\begin{aligned} \Phi_{apn} &= \frac{4\pi N_p N_c K_{dpn}}{m_n (R_s - R_i)} \int_{R_i}^{R_s} r \{ [F_{Aan}(m_n r) + a_{\text{Ian}}] \\ &\quad BI_1(m_n r) + [-F_{Ban}(m_n r) + b_{\text{Ian}}] BK_1(m_n r) \} dr \end{aligned} \quad (57)$$

and $N_c = N_w/2N_p$ is the number of series turns per phase per pole. The self-inductance of the winding is, therefore, given by

$$\begin{aligned} L_s &= \frac{\psi_{wap}}{J_0 \tau_w (R_s - R_i) / N_c} \\ &= \frac{\pi N_w^2}{N_p \tau_w (R_s - R_i)^2} \sum_{n=1,2,\dots}^{\infty} \frac{k_l K_{dpn}}{m_n} \end{aligned} \quad (58)$$

where

$$\begin{aligned} k_l &= \int_{R_i}^{R_s} r \{ [F'_{anp}(m_n r) + a'_{\text{Ian}}] BI_1(m_n r) \\ &\quad + [-F'_{Ban}(m_n r) + b'_{\text{Ian}}] BK_1(m_n r) \} dr \end{aligned} \quad (59)$$

and $F'_{Aan}(\bullet)$, $F'_{Ban}(\bullet)$, a'_{Ian} , b'_{Ian} , a'_{IIan} , and b'_{IIan} are calculated, respectively, from $F_{Aan}(\bullet)$, $F_{Ban}(\bullet)$, a_{Ian} , b_{Ian} , a_{IIan} , and b_{IIan} by substituting $J_0 = 1$. The mutual inductance M_{ij} between phases i and j ($i \neq j$) separated by an axial distance τ_{ij} can be similarly deduced, and is given by

$$M_{ij} = \frac{\pi N_w^2}{N_p \tau_w (R_s - R_i)^2} \sum_{n=1,2,\dots}^{\infty} \frac{k_l K_{dpn}}{m_n} \cos m_n \tau_{ij}. \quad (60)$$

Several observations can be made from the foregoing, viz.

$$\begin{cases} \left[\frac{\partial}{\partial z} \left(\frac{1}{r} \frac{\partial}{\partial z} (r A_{\text{I}\theta}) \right) + \frac{\partial}{\partial r} \left(\frac{1}{r} \frac{\partial}{\partial r} (r A_{\text{I}\theta}) \right) \right] = -\mu_0 \sum_{n=1}^{\infty} J_n \sin m_n z & \text{in the winding area} \\ \left[\frac{\partial}{\partial z} \left(\frac{1}{r} \frac{\partial}{\partial z} (r A_{\text{II}\theta}) \right) + \frac{\partial}{\partial r} \left(\frac{1}{r} \frac{\partial}{\partial r} (r A_{\text{II}\theta}) \right) \right] = 0 & \text{in the airgap/magnets} \end{cases} \quad (51)$$

- 1) For slotted armatures, the effect of slotting may be accounted for by the use of a Carter coefficient, as before. Therefore, the armature reaction field may be obtained by solving the following equation:

$$\frac{\partial}{\partial z} \left(\frac{1}{r} \frac{\partial}{\partial z} (rA_\theta) \right) + \frac{\partial}{\partial r} \left(\frac{1}{r} \frac{\partial}{\partial r} (rA_\theta) \right) = 0$$

in the airgap/magnets (61)

subject to the boundary conditions

$$B_z|_{r=R_r} = 0; \quad H_z|_{r=R_{ie}} = \sum_{n=1,2,\dots}^{\infty} J_n \sin m_n z. \quad (62)$$

Expressions for the winding self- and mutual-inductances can similarly be deduced from the field solution.

- 2) The results in this section are applicable to radially-magnetized and Halbach cylinder machine topologies. For the axially-magnetized machine topology, although an analytical solution for the armature reaction field is possible, the analysis is considerably more complex. Further, the self- and mutual-winding inductances will be position dependant due to the presence of the iron pole pieces.

V. CONCLUSION

A general framework for the analysis and design of a class of tubular, linear permanent magnet machines has been developed. Analytical expressions for the open-circuit and armature reaction fields have been established for radially, axially, and Halbach magnetized machine topologies, and expressions for the force, emf, and self- and mutual-winding inductances have been derived. The effects of slotting and fringing have also been taken into account. The analyses have been validated by finite element calculations and measurements. The analytical tools should, therefore, be useful for comparative studies, design optimization, and dynamic modeling of a variety of tubular linear permanent magnet machines.

APPENDIX A

DEFINITION OF $F_{An}(\bullet)$, $F_{Bn}(\bullet)$, a_{In} , b_{In} , a_{IIIn} , AND b_{IIIn}

Let

$$\begin{aligned} c_{1n} &= BI_0(m_n R_s); & c_{2n} &= BK_0(m_n R_s) \\ c_{3n} &= BI_0(m_n R_r); & c_{4n} &= BK_0(m_n R_r) \\ c_{5n} &= BI_0(m_n R_m); & c_{6n} &= BK_0(m_n R_m) \\ c_{7n} &= BI_1(m_n R_m); & c_{8n} &= BK_1(m_n R_m) \end{aligned} \quad (A.1)$$

$$F_{An}(m_n r) = \frac{P_n}{m_n} \int_{m_n R_r}^{m_n r} \frac{BK_1(x) dx}{BI_1(x)BK_0(x) + BK_1(x)BI_0(x)} \quad (A.2)$$

$$F_{Bn}(m_n r) = \frac{P_n}{m_n} \int_{m_n R_r}^{m_n r} \frac{BI_1(x) dx}{BI_1(x)BK_0(x) + BK_1(x)BI_0(x)} \quad (A.3)$$

a_{In} and a_{IIIn} are solutions of the following linear equations:

$$\begin{aligned} & \left[\begin{array}{c} \mu_r \left(\frac{c_{5n}}{c_{6n}} - \frac{c_{1n}}{c_{2n}} \right) - \left(\frac{c_{5n}}{c_{6n}} - \frac{c_{3n}}{c_{4n}} \right) \\ \left(\frac{c_{7n}}{c_{8n}} + \frac{c_{1n}}{c_{2n}} \right) - \left(\frac{c_{7n}}{c_{8n}} + \frac{c_{3n}}{c_{4n}} \right) \end{array} \right] \begin{bmatrix} a_{In} \\ a_{IIIn} \end{bmatrix} \\ & = \left[\begin{array}{c} F_{An}(m_n R_m) \frac{c_{5n}}{c_{6n}} + F_{Bn}(m_n R_m) \\ F_{An}(m_n R_m) \frac{c_{7n}}{c_{8n}} - F_{Bn}(m_n R_m) \end{array} \right] \end{aligned} \quad (A.4)$$

and

$$b_{In} = \frac{c_{1n}}{c_{2n}} a_{In}; \quad b_{IIIn} = \frac{c_{3n}}{c_{4n}} a_{IIIn}. \quad (A.5)$$

APPENDIX B

DEFINITION OF $F_{Ap}(\bullet)$, $F_{Bp}(\bullet)$, a_{IP} , b_{IP} , a_{IIp} , AND b_{IIp}

Let

$$\begin{aligned} c_1 &= BI_0(pR_s); & c_2 &= BK_0(pR_s); & c_3 &= BI_0(pR_r) \\ c_4 &= BK_0(pR_r); & c_5 &= BI_0(pR_m); & c_6 &= BK_0(pR_m) \\ c_7 &= BI_1(pR_m); & c_8 &= BK_1(pR_m). \end{aligned} \quad (A.6)$$

$$F_{Ap}(pr) = B_{rem} \int_{pR_r}^{pr} \frac{BK_1(x) dx}{BI_1(x)BK_0(x) + BK_1(x)BI_0(x)}. \quad (A.7)$$

$$F_{Bp}(pr) = B_{rem} \int_{pR_r}^{pr} \frac{BI_1(x) dx}{BI_1(x)BK_0(x) + BK_1(x)BI_0(x)}. \quad (A.8)$$

a_{IP} and a_{IIp} are solutions of the following linear equations:

$$\begin{aligned} & \left[\begin{array}{c} \mu_r \left(\frac{c_5}{c_6} - \frac{c_1}{c_2} \right) - \left(\frac{c_5}{c_6} - \frac{c_3}{c_4} \right) \\ \left(\frac{c_7}{c_8} + \frac{c_1}{c_2} \right) - \left(\frac{c_7}{c_8} + \frac{c_3}{c_4} \right) \end{array} \right] \begin{bmatrix} a_{IP} \\ a_{IIp} \end{bmatrix} \\ & = \left[\begin{array}{c} F_{Ap}(pR_m) \frac{c_5}{c_6} + F_{Bp}(pR_m) \pm \frac{B_{rem}}{c_6} \\ F_{Ap}(pR_m) \frac{c_7}{c_8} - F_{Bp}(pR_m) \end{array} \right] \end{aligned} \quad (A.9)$$

and

$$b_{IP} = \frac{c_1}{c_2} a_{IP}; \quad b_{IIp} = \frac{c_3}{c_4} a_{IIp} \quad (A.10)$$

where the positive and negative signs preceding B_{rem}/c_6 correspond to internal and external magnet machine topologies, respectively.

APPENDIX C

DEFINITION OF a'_{IP} , a'_{IIp} , b'_{IP} , AND b'_{IIp}

$$\begin{aligned} c_{1p} &= BI_0(pR_m); & c_{2p} &= BK_0(pR_m); & c_{3p} &= BI_1(pR_m) \\ c_{4p} &= BK_1(pR_m); & c_{5p} &= BI_0(pR_r); & c_{6p} &= BK_0(pR_r) \\ c_{7p} &= BI_1(pR_r); & c_{8p} &= BK_1(pR_r) \end{aligned} \quad (A.11)$$

$$a'_{IP} = [F_{Ap}(pR_m) + B_{rem} c_{4p} / (c_{1p} c_{4p} + c_{2p} c_{3p})] \quad (A.12)$$

$$b'_{IP} = [-B_{rem} c_{7p} / (c_{5p} c_{8p} + c_{6p} c_{7p})] \quad (A.13)$$

$$a'_{IIp} = a'_{IP} + \frac{c_{6p}}{c_{7p}} b'_{IP} \quad (A.14)$$

$$a'_{IP} = [-F_{Ap}(pR_m) + a'_{IIp}] \frac{c_{3p}}{c_{4p}} + [F_{Bp}(pR_m) + b'_{IIp}]. \quad (A.15)$$

APPENDIX D

DEFINITION OF a'_{In} , b'_{In} , a'_{IIj} , AND B_0

Let

$$M_n = \frac{4B_{rem} \sin(2n-1)\frac{\pi}{2}\alpha_p}{\pi\mu_0 (2n-1)}$$

$$Q_n = \frac{4 \sin(2n-1)\frac{\pi}{2}\alpha_p}{\pi\mu_0 (2n-1)} \quad (A.16)$$

$$u = \left(\frac{2j}{\tau_m} + \frac{2n-1}{\tau_p}\right)\frac{\pi\tau_m}{2}; \quad v = \left(\frac{2j}{\tau_m} - \frac{2n-1}{\tau_p}\right)\frac{\pi\tau_m}{2} \quad (A.17)$$

$$R_{IIjn} = \frac{1}{\mu_r} BI_0(q_j R_m) \alpha_p \left(\frac{\sin u}{u} + \frac{\sin v}{v}\right) \quad (A.18)$$

$$D_{In} = c_{5n} - \frac{c_{1n}}{2c_n} c_{6n}; \quad D_{IIj} = BI_1(q_j R_m) \quad (A.19)$$

$$R_{Ijn} = \left(c_{7n} + \frac{c_{1n} c_{8n}}{c_{2n}}\right) \left(\frac{\sin v}{v} - \frac{\sin u}{u}\right) \quad (A.20)$$

$$R_{In} = \left(c_{7n} + \frac{c_{1n} c_{8n}}{c_{2n}}\right) \frac{\cos \frac{\tau_m m_n}{2}}{m_n}; \quad R_{IIj} = D_{IIj} \frac{\cos \frac{\tau_m q_j}{2}}{q_j}. \quad (A.21)$$

Then a'_{In} , a'_{IIj} , and B_0 are solutions of the following $(N_E + J_E + 1) \times (N_E + J_E + 1)$ linear equations:

$$D_{In} a'_{In} - \sum_{j=1}^{J_E} R_{IIjn} a'_{IIj} - Q_n B_0 = -\frac{\mu_0}{\mu_r} M_n$$

$$\sum_{n=1}^{N_E} R_{Ijn} a'_{In} - D_{IIj} a'_{IIj} = 0 \quad (A.22)$$

$$\sum_{n=1}^{N_E} R_{In} a'_{In} - \sum_{j=1}^{J_E} R_{IIj} a'_{IIj} - \frac{R_m}{2} B_0 = 0$$

and

$$b'_{In} = (c_{1n}/c_{2n}) a'_{In} \quad (A.23)$$

where N_E and J_E are the numbers of the harmonic terms used for the calculation of the flux density in regions I and II, respectively.

If, however, $\tau_m = \tau_p$, i.e., the thickness of the iron pole-pieces is zero, then, $q_j = m_n$, $B_0 = 0$, and a'_{In} , b'_{In} , a'_{IIj} are given by

$$a'_{In} = \frac{\frac{4B_{rem}}{(2n-1)\pi} \sin(2n-1)\frac{\pi}{2}}{\left[\frac{c_{1n}}{c_{2n}} \left(\frac{c_{8n}}{c_{7n}} + \mu_r \frac{c_{6n}}{c_{5n}}\right) - (\mu_r - 1)\right] c_{5n}}$$

$$b'_{In} = \frac{c_{1n}}{c_{2n}} a'_{In} \quad (A.24)$$

$$a'_{IIj} = \left(1 + \frac{c_{1n} c_{8n}}{c_{2n} c_{7n}}\right) a'_{In}.$$

APPENDIX E

DEFINITION OF $F_{Aan}(\bullet)$, $F_{Ban}(\bullet)$, a_{Ian} , b_{Ian} , a_{IIan} , AND b_{IIan}

$$F_{Aan}(m_n r) = -\frac{\mu_0 J_n}{m_n} \int_{m_n R_i}^{m_n r} \frac{BK_1(x) dx}{BI_1(x)BK_0(x) + BK_1(x)BI_0(x)} \quad (A.25)$$

$$F_{Ban}(m_n r) = -\frac{\mu_0 J_n}{m_n} \int_{m_n R_i}^{m_n r} \frac{BI_1(x) dx}{BI_1(x)BK_0(x) + BK_1(x)BI_0(x)} \quad (A.26)$$

$$\begin{cases} a_{Ian} = -[F_{Aan}(m_n R_s) + F_{Ban}(m_n R_s) c_{2n}/c_{1n}] \\ \quad \quad \quad [1 - c_{2n} c_{3n}/(c_{1n} c_{4n})] \\ b_{Ian} = (c_{3n}/c_{4n}) a_{Ian} \\ a_{IIan} = a_{Ian} \\ b_{IIan} = b_{Ian}. \end{cases} \quad (A.27)$$

ACKNOWLEDGMENT

The authors would like to thank Dr. Z. Q. Zhu and P. J. Hor for providing the design details and measured flux-linkage waveform of the slotted linear motor.

REFERENCES

- [1] R. E. Clark, D. S. Smith, P. H. Mellor, and D. Howe, "Design optimization of moving-magnet actuators for reciprocating electro-mechanical systems," *IEEE Trans. Magn.*, vol. 31, pp. 3746–48, Nov. 1995.
- [2] M. A. White, K. Colenbrander, R. W. Olan, and L. B. Penswick, "Generators that won't wear out," *Mech. Eng.*, vol. 118, no. 2, pp. 92–96, 1996.
- [3] M. Watada, K. Yanashima, Y. Oishi, and D. Ebihara, "Improvement on characteristics of linear oscillatory actuator for artificial hearts," *IEEE Trans. Magn.*, vol. 29, pp. 3361–3363, Nov. 1993.
- [4] J. F. Eastham, "Novel synchronous machines: linear and disc," *Proc. Inst. Elect. Eng.*, vol. B-137, pp. 49–58, 1990.
- [5] I. Boldea and S. A. Nasar, *Linear Electric Actuators and Generators*. Cambridge, U.K.: Cambridge Univ. Press, 1997.
- [6] T. Mizuno and H. Yamada, "Magnetic circuit analysis of a linear synchronous motor with permanent magnets," *IEEE Trans. Magn.*, vol. 28, pp. 3027–3029, Sept. 1992.
- [7] R. Akmese and J. F. Eastham, "Dynamic performance of a brushless DC tubular drive system," *IEEE Trans. Magn.*, vol. 25, pp. 3269–3271, Sept. 1989.
- [8] A. Basak and G. H. Shirkoohi, "Computation of magnetic field in D.C. brushless linear motors built with NdFeB magnets," *IEEE Trans. Magn.*, vol. 26, pp. 948–950, Mar. 1990.
- [9] G. Xiong and S. A. Nasar, "Analysis of fields and forces in a permanent magnet linear synchronous machine based on the concept of magnetic charge," *IEEE Trans. Magn.*, vol. 25, pp. 2713–2719, May 1989.
- [10] Z. J. Liu, A. Vourdas, and K. J. Binns, "Magnetic field and eddy current losses in linear and rotating permanent magnet machines with a large number of poles," *Proc. Inst. Elect. Eng.*, vol. A-138, no. 6, pp. 289–294, 1991.
- [11] D. L. Trumper, W. Kim, and M. E. Williams, "Design and analysis framework for linear permanent magnet machines," *IEEE Trans. Ind. Applicat.*, vol. 32, no. 2, pp. 371–379, 1996.
- [12] Y. He, Z. Q. Zhu, and D. Howe, "A PWM controlled linear servo system for friction welding," in *Proc. 2nd Int Conf. Elect. Mach. (CICEM'95)*, Hangzhou, China, 1995, vol. A 2.3, pp. 51–55.
- [13] Z. Q. Zhu, Z. P. Xia, D. Howe, and P. H. Mellor, "Reduction of cogging force in slotless linear permanent magnet motors," *Proc. Inst. Elect. Eng.*, vol. B-144, no. 4, pp. 227–282, 1997.
- [14] K. Atallah and D. Howe, "Design and analysis of multi-pole Halbach (self-shielding) cylinder brushless permanent magnet machines," in *Proc. EMD'97*, Cambridge, U.K., 1997, pp. 376–380.
- [15] Q. Gu and H. Gao, "Effect of slotting in PM electrical machines," *Elect. Mach. Power Syst.*, vol. 10, no. 2, pp. 273–284, 1985.
- [16] Q. Gu and H. Gao, "The fringing effect in PM electric machines," *Elect. Mach. Power Syst.*, vol. 11, no. 2, pp. 159–169, 1986.
- [17] Z. Q. Zhu and D. Howe, "Magnet design considerations for electrical machines equipped with surface-mounted permanent magnets," in *Proc. 13th Int. Workshop Rare-earth Permanent Magnets Applicat.*, 1994, pp. 151–160.
- [18] Z. Q. Zhu, P. J. Hor, D. Howe, and J. R. Jones, "Calculation of cogging force in a novel slotted linear tubular brushless permanent magnet motor," in *Proc. INTERMAG-97*, New Orleans, LA, 1997.

Jiabin Wang (M'96) was born in Jiangsu Province, China, in 1958. He received the B.Eng. and M.Sc. degrees from Jiangsu University of Technology, China, in 1982 and 1986, respectively, and the Ph.D. from the University of East London, U.K., in 1996, all in electrical and electronic engineering.

From 1986 to 1991 he worked in the Department of Electrical Engineering, Jiangsu University of Technology and was appointed a Lecturer in 1987 and Associated Professor in 1990. He was a Postdoctoral Research Associate at the University of Sheffield from 1996 to 1997 and is currently a Senior Lecturer at the University of East London. His research interests range from motion control to electromagnetic devices and their associated drives.

Geraint W. Jewell was born in Neath, Wales, in 1966. He received the B.Eng. and Ph.D. degrees from the University of Sheffield, U.K., in 1988 and 1992, respectively.

He is currently a Lecturer in the Department of Electronic and Electrical Engineering at the University of Sheffield, a position he has held since 1994. His research interests are related to a wide range of electromagnetic devices including linear and spherical actuators, magnetic bearings, bearingless machines, high speed machines, and multipole impulse magnetizing fixtures.

David Howe was born in Sheffield, England, in 1943. He received the B.Tech and M.Sc. degrees from the University of Bradford, U.K., and the Ph.D. degree from the University of Southampton, U.K.

Before joining the University of Sheffield, U.K., he held posts with Northern Engineering Industries Ltd., Newcastle-upon-Tyne, U.K., and Brunel University, Uxbridge, Middlesex, U.K. He is currently Lucas Professor of Electrical Engineering at Sheffield, where his research interests range from electric vehicles to multi-axis drives for high-speed manufacturing. He is also Co-Founder and Director of Magnetic Systems Technology Ltd.